Title	Impact of self-attraction and loading on the annual cycle in sea level.
Author(s)	Tamisiea, Mark E.; Hill, Emma M.; Ponte, R. M.; Davis, James L.; Velicogna, I.; Vinogradova, N. T.
Citation	Tamisiea, M. E., Hill, E. M., Ponte, R. M., Davis, J. L., Velicogna, I., & Vinogradova, N. T. (2010). Impact of self-attraction and loading on the annual cycle in sea level. Journal of Geophysical Research, 115, 1-15.
Date	2010
URL	http://hdl.handle.net/10220/8209
Rights	© 2010 by the American Geophysical Union (AGU). This paper was published in Journal of Geophysical Research and is made available as an electronic reprint (preprint) with permission of AGU. The paper can be found at DOI: [http://dx.doi.org/10.1029/2009JC005687]. One print or electronic copy may be made for personal use only. Systematic or multiple reproduction, distribution to multiple locations via electronic or other means, duplication of any material in this paper for a fee or for commercial purposes, or modification of the content of the paper is prohibited and is subject to penalties under law.

JOURNAL OF GEOPHYSICAL RESEARCH, VOL. 115, C07004, doi:10.1029/2009JC005687, 2010

Impact of self-attraction and loading on the annual cycle in sea level

M. E. Tamisiea,[1] E. M. Hill,[2] R. M. Ponte,[3] J. L. Davis,[2] I. Velicogna,[4] and N. T. Vinogradova[3]

Received 5 August 2009; revised 23 November 2009; accepted 23 February 2010; published 7 July 2010.

[1] The annual exchange of water between the continents and oceans is observed by GPS, gravimetry, and altimetry. However, the global average amplitude of this annual cycle (observed amplitude of ~8 mm) is not representative of the effects that would be observed at individual tide gauges or at ocean bottom pressure recorders because of self-attraction and loading effects (SAL). In this paper, we examine the spatial variation of sea level change caused by the three main components that load the Earth and contribute to the water cycle: hydrology (including snow), the atmosphere, and the dynamic ocean. The SAL effects cause annual amplitudes at tide gauges (modeled here with a global average of ~9 mm) to vary from less than 2 mm to more than 18 mm. We find a variance reduction (global average of 3 to 4%) after removing the modeled time series from a global set of tide gauges. We conclude that SAL effects are significant in places (e.g., the south central Pacific and coastal regions in Southeast Asia and west central Africa) and should be considered when interpreting these data sets and using them to constrain ocean circulation models.

Citation: Tamisiea, M. E., E. M. Hill, R. M. Ponte, J. L. Davis, I. Velicogna, and N. T. Vinogradova (2010), Impact of self-attraction and loading on the annual cycle in sea level, *J. Geophys. Res.*, *115*, C07004, doi:10.1029/2009JC005687.

1. Introduction

[2] The annual cycle of sea level measured by tide gauges [e.g., *Tsimplis and Woodworth*, 1994] is a result of changes in ocean density, dynamic ocean effects, and changes in total ocean mass. The total mass change is a well-observed phenomena [e.g., *Blewitt and Clarke*, 2003; *Chambers et al.*, 2004; *Wu et al.*, 2006], equivalent to a global average sea level amplitude of about 8 mm. Recently, this exchange has played an important role in the comparison of three ocean-observing systems: Jason-1, the Gravity Recovery and Climate Experiment (GRACE), and Argo [*Willis et al.*, 2008; *Leuliette and Miller*, 2009; *Cazenave et al.*, 2009]. In an ocean model that conserved mass, this global mass signal would produce uniform sea level changes around the globe. However, that is ignoring the gravitational and self-attraction and loading (SAL) effects produced by the global redistribution of mass. These changing loads, particularly over continents, produce a spatial pattern of sea level change that is far from uniform [e.g., *Clarke et al.*, 2005]. In this paper, we focus on how this water will be distributed, and the ability of the resulting geographically varying sea level predictions to better reconcile observations with ocean model predictions at tide gauges.

[3] Seasonally, water mass moves among the atmosphere, oceans, and continents. The largest component of this exchange, the annual variation of water stored on land, is nonuniformly distributed about the continents (e.g., see Figure 1). This nonuniform variation of mass will in turn load the Earth and cause geographically varying changes to the geoid (the equipotential surface that would describe the sea surface if the ocean was static) and the crust [e.g., *Farrell and Clark*, 1976]. It has long been known that any land-based system, such as ice sheets or glaciers, that exchanges mass with the oceans will cause a nonuniform change in sea level [*Farrell and Clark*, 1976; *Clark and Primus*, 1987; *Nakiboglu and Lambeck*, 1991; *Conrad and Hager*, 1997; *Mitrovica et al.*, 2001; *Plag and Jüttner*, 2001; *Tamisiea et al.*, 2001], independent of any dynamic effects caused by the freshwater flux. In the literature on ocean tides [e.g., *Ray*, 1998], these effects are termed self-attraction and loading (SAL). Here, we note that we are also including in the SAL term the variation in the ocean mass due to the exchange with the continents.

[4] Figure 2 is a cartoon illustrating the local effects on sea level as additional water is stored in a river basin. Figure 2a shows the initial state of the system during a low point in the annual water storage cycle. The box represents a river basin that can store additional water. As water accumulates in the river basin (Figure 2b) the relative sea level, as would be measured by a tide gauge, is locally impacted in two ways

[1] National Oceanography Centre, Liverpool, UK.
[2] Harvard-Smithsonian Center for Astrophysics, Cambridge, Massachusetts, USA.
[3] Atmospheric and Environmental Research, Inc., Lexington, Massachusetts, USA.
[4] School of Physical Sciences, University of California, Irvine, California, USA.

0148-0227/10/2009JC005687

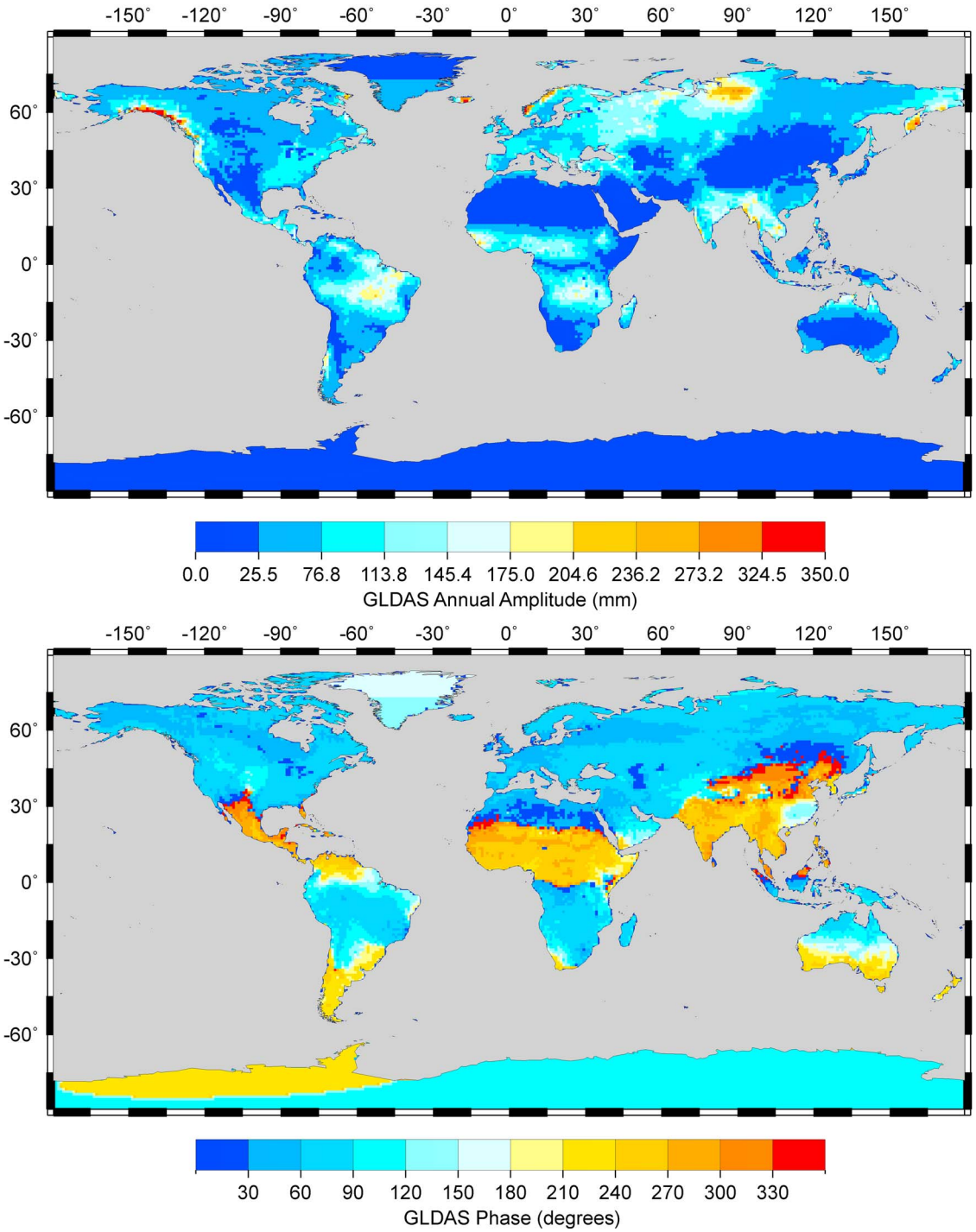

Figure 1. Annual-cycle (top) amplitude and (bottom) phase of the GLDAS/Noah model over the period 1980–1997. Note that the divisions in the amplitude color bar are not regular. The results from Greenland are explicitly excluded from the model (and there are no results for Antarctica). Instead, an amplitude and phase derived from GRACE data from April 2002 through September 2008 are substituted.

(a global effect is discussed below). First, the additional mass of the water depresses the crust beneath the river basin. Because the tide gauge is attached to the crust, it also is depressed and thus measures a sea level rise. In addition, the extra mass present in the river basin creates a gravitational attraction, or tide, on the nearby ocean, causing additional water to be pulled up to the region near the basin. This lifting of the sea surface near the river basin also contributes to the sea level rise at the tide gauge. Combined, these near field effects also contribute to an increased load in the region compared to that which would be expected from simply assuming an average over the whole ocean. In the following analysis, we assume that the Earth's response to the changing continental loads is instantaneous (i.e., elastic). Thus when

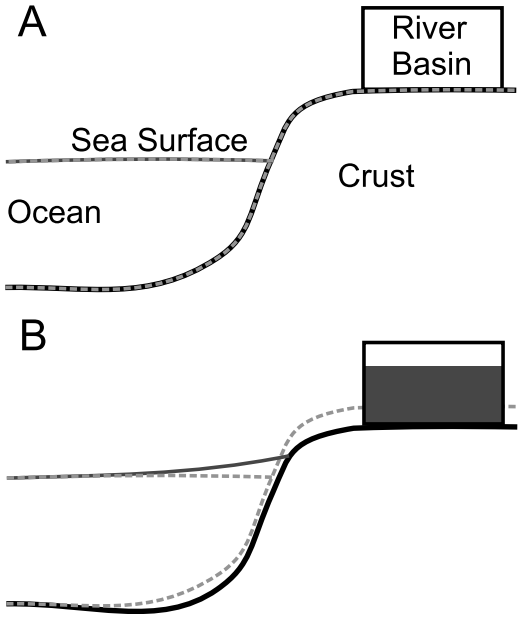

Figure 2. Cartoon illustrating the local impact of continental water storage on sea level. (a) Initial configuration of the sea surface and crust prior to loading. (b) Sea surface and crust at the maximum of water-storage cycle in a river basin. The initial configuration is indicated by the dashed lines. After the river basin drains, the sea surface and crust will return to positions shown in Figure 2a.

the additional stored water leaves the basin, the system will return to the configuration shown in Figure 2a.

[5] Simultaneous to the local effects illustrated in Figure 2, the global average of ocean mass, and thus the globally averaged sea level, varies as water is exchanged with the continents. Therefore the overall sea level change at any given point is the relative balance between the local effects of Figure 2 and the globally averaged change. This balance will be explicitly illustrated in section 5.

[6] *Clarke et al.* [2005] used hydrological and atmospheric data sets combined with ocean model output to approximate the three largest components of the annual global water cycle. In particular, they found that taking into account the SAL effects significantly impacts estimates of the annual variation of the geocenter (the motion of the figure of the Earth relative to the center of mass of the whole Earth.) We will follow the same approach of using data sets to model the water cycle. However, as we are examining local effects of SAL through tide gauge (and later bottom pressure) measurements, we expand these models to higher spherical harmonic degree and order than *Clarke et al.* [2005].

[7] The majority of observed variations in sea level are caused by the ocean's response to driving forces and fluxes. *Hill et al.* [2007, hereafter HPD] investigated the ability of an ocean model and calculated inverted barometer (IB) ocean response to atmospheric pressure [*Ponte*, 2006] to explain temporal variability in tide gauge records. Specifically, HPD examined the reduction in the variance of the observed time series after removing their estimates. Even after removing the IB effect and a scaled ocean model (the variance at a few sites was significantly improved by fitting an admittance parameter to the ocean model), there remained a significant annual cycle in many of the time series. If an annual cycle is simultaneously fit to the time series, along with the admittance (scaling) parameter for the ocean model, the variance is reduced by 71%. The global average of the residual annual cycle from this procedure (at a set of 380 tide gauges) is 35 ± 15 mm [HPD]. Thus by simply comparing this estimated average amplitude (~35 mm) with the observed ocean mass exchange (~8 mm), the ocean-continent-atmosphere exchange could account for ~25% of the residual amplitude.

[8] Recent observations of bottom pressure from GRACE give another motivation for examining the SAL effects [e.g., *Ponte et al.*, 2007]. In particular, the ratio of SAL effects to the dynamic ocean signal should be larger when considering ocean bottom pressure, which typically has smaller annual variations at a given location than sea level [*Vinogradov et al.*, 2008]. Currently, SAL effects are not represented by many ocean models that are used to estimate bottom pressure variations, which, along with other missing model physics, can explain poor model/data agreement [*Vinogradova et al.*, 2010].

[9] Below, we detail the method used to calculate the SAL effect on sea level and bottom pressure caused by the global water cycle. In section 3 we give more details on each of the components we use in modeling the water cycle, followed by a short comment on comparing the model results to observations. Section 5 details the SAL effects from each of the loads, and we conclude by comparing the results to residual tide gauge time series derived in HPD.

2. Method

[10] When investigating the exchange and spatial distribution of water between the oceans and the continents, we start with a set of known loads given by data sets or models: hydrology, atmospheric pressure, and dynamic ocean bottom pressure. Individually, neither hydrology nor atmospheric pressure model results prescribe the source or sink of water as its global average changes. In total, however, water mass should be conserved. Thus the global average of these known loads must be balanced by a water load added or subtracted from the ocean. The spatial distribution of this additional water load over the ocean will be impacted by the related crustal displacement and gravitational changes discussed in the Introduction. It is this spatial distribution we will calculate below.

[11] We use a formalism developed to describe variations in sea level during the last ice age [e.g., *Farrell and Clark*, 1976; *Mitrovica and Peltier*, 1991; *Mitrovica and Milne*, 2003], which assumes that all changes in the sea surface and water distribution will be caused by changes to the geoid, the Earth's crust, and variation in the water volume of the oceans. Thus SAL effects are assumed to give rise to a purely static adjustment in the ocean, with no dynamics being considered here, except to the extent that the dynamic part of ocean bottom pressure represents a mass variation which acts as an input to the SAL calculations. The following discussion follows closely the more detailed (and general) discussion of *Kendall et al.* [2005] and is meant to give a review of those results and how the relevant equations simplify for short-time-scale sea level variations considered

here. In addition, the discussion serves to define the terms used throughout the paper.

[12] The sea level equation, introduced in the classic paper by *Farrell and Clark* [1976], globally defines relative sea level (or equivalently ocean thickness), SL, as the difference between the geoid (defined here as an equipotential surface whose value can change with time), G, and the crust, R, at time t_j:

$$SL(\theta,\phi,t_j) = G(\theta,\phi,t_j) - R(\theta,\phi,t_j) \tag{1}$$

where θ is the colatitude and ϕ is longitude. It should be noted that G is the sea surface in the absence of ocean dynamics and its value and position will change with time. With this definition, the ocean height, S, then corresponds to a projection of the SL onto the ocean function, $C(\theta, \phi, t_j)$, which is globally defined as 1 over the oceans ($SL \geq 0$) and 0 over land ($SL < 0$):

$$S(\theta,\phi,t_j) = SL(\theta,\phi,t_j)\cdot C(\theta,\phi,t_j) \tag{2}$$

[13] Given the relatively short timescale of the loading, we assume that the Earth will deform elastically and will return to its initial state once the loads are removed. This also implies that the system has no memory, and thus the loading history is not important. In the context of annual variation of water loads, this is a reasonable assumption. Letting Δ represent the difference in a quantity between t_j and t_0, i.e., $\Delta R(\theta, \phi, t_j) = R(\theta, \phi, t_j) - R(\theta, \phi, t_0)$, then equations (1) and (2) can be expressed as

$$\Delta SL(\theta,\phi,t_j) = \Delta G(\theta,\phi,t_j) - \Delta R(\theta,\phi,t_j) \tag{3}$$

$$\Delta S(\theta,\phi,t_j) = \Delta SL(\theta,\phi,t_j)\cdot C(\theta,\phi) \tag{4}$$

These changes are the contribution of the prescribed loading and associated ocean load to tide gauge measurements, $\Delta SL(\theta, \phi, t_j)$, or altimetry measurements, $\Delta G(\theta, \phi, t_j)$. Note that equation (4) assumes the changes in sea level are small in comparison to the resolution of the initial topography model, i.e., the ocean function $C(\theta, \phi)$ is independent of time (see Appendix A).

[14] It should be noted that $\Delta G(\theta, \phi, t_j)$ does not correspond directly with changes in the classic definition of geoid height, $\Delta\mathcal{G}(\theta, \phi, t_j)$, since the equipotential value corresponding to the sea surface may change over time (a change from time t_0 that we denote by $\Delta\Phi(t_j)$) both due to changes in overall water volume, as well as changes in the ocean basin shape. Thus $\Delta G(\theta, \phi, t_j)$ can be represented by

$$\Delta G(\theta,\phi,t_j) = \Delta\mathcal{G}(\theta,\phi,t_j) + \Delta\Phi(t_j)/g \tag{5}$$

where g is the gravitational acceleration. Note that $\Delta\Phi(t_j)$ does not depend upon position and will be calculated via conservation of mass. Finally, we define $\Delta\mathcal{SL}$ as

$$\begin{aligned}\Delta SL(\theta,\phi,t_j) &= \left[\Delta\mathcal{G}(\theta,\phi,t_j) - \Delta R(\theta,\phi,t_j)\right] + \Delta\Phi(t_j)/g \\ &= \Delta\mathcal{SL}(\theta,\phi,t_j) + \Delta\Phi(t_j)/g\end{aligned} \tag{6}$$

$$\Delta S(\theta,\phi,t_j) = \left[\Delta\mathcal{SL}(\theta,\phi,t_j) + \Delta\Phi(t_j)/g\right]\cdot C(\theta,\phi) \tag{7}$$

This expression for the associated ocean load is an integral equation because the terms in the square brackets of equation (7) depend upon ΔS. Thus these equations are generally solved iteratively.

[15] From here on, we will drop the explicit dependence upon θ and ϕ, and time $t = t_j$ will be represented with a subscript j. If we introduce a superscript i that represents the iteration number, then we can write

$$\Delta S_j^i = \left[\Delta\mathcal{SL}_j^{i-1}(\Delta AL_j; \Delta S_j^{i-1}) + \Delta\Phi_j^{i-1}/g\right]\cdot C \tag{8}$$

$$\begin{aligned}\Delta\Phi_j^{i-1}/g = &-\int\int_\Omega \left[\Delta AL_j + \Delta\mathcal{SL}_j^{i-1}(\Delta AL_j; \Delta S_j^{i-1})\cdot C\right] d\Omega \\ &\Big/ \int\int_\Omega C\, d\Omega\end{aligned} \tag{9}$$

where ΔAL_j describes the total applied load at time $t = t_j$, and we have explicitly introduced the dependence of $\Delta\mathcal{SL}$ on the applied load and inferred ocean load following the SAL adjustment. Equation (9) is derived by integrating equation (8) over the Earth's surface and is a statement of the global conservation of water mass. The total inferred ocean load, the surface integral of ΔS, must balance the total of the applied loads. For the initial guess, $i = 0$, we assume that $\Delta\mathcal{SL}_j^{-1} = 0$. This assumption, when substituted into equations (8) and (9), gives a spatially uniform layer over the oceans that balances the global average of the applied loads.

[16] If these equations are expanded via spherical harmonics, then the solid Earth deformation and changes in the geoid can be expressed in terms of the load (h_l^L and k_l^L) Love numbers, where l is the spherical harmonic degree. These Love numbers represent how the Earth would deform and how its potential field would change in response to a load of a certain wavelength. Thus these factors capture the physics represented in Figure 2. In general, the expansion of some quantity, e.g., $\Delta\mathcal{SL}_j^i$, is given by

$$\begin{aligned}\Delta\mathcal{SL}^i(\theta,\phi,t_j) = \Delta\mathcal{SL}_j^i(\theta,\phi) &= \sum_{l=0}^{N}\sum_{m=-l}^{l}\left[\Delta\mathcal{SL}_{lm}(t_j)\right]^i Y_{lm}(\theta,\phi) \\ &= \sum_{l,m}\left[\Delta\mathcal{SL}_{lm}(t_j)\right]^i Y_{lm}(\theta,\phi)\end{aligned} \tag{10}$$

where l and m are the spherical harmonic degree and order. Given this notation, we can express each l, m coefficient of $\Delta\mathcal{SL}$ as

$$\left[\Delta\mathcal{SL}_{lm}(t_j)\right]^{i-1} = \frac{3\rho_w(1+k_l^L-h_l^L)}{\rho_e(2l+1)}\left(\Delta AL_{lm}(t_j) + \left[\Delta S_{lm}(t_j)\right]^{i-1}\right) \tag{11}$$

where ρ_e is the average density of the Earth and ρ_w is the density for water. A convenient feature of spherical harmonics is that the $l = 0$, $m = 0$ coefficient represents the average of the field over the entire Earth, which makes the conservation of mass equation, equation (9), straightforward

to solve. Expanding in terms of spherical harmonic coefficients, equations (8) and (9) reduce to

$$[\Delta S_{lm}(t_j)]^i = [RO_{lm}(t_j)]^{i-1} + [\Delta\Phi/g]^{i-1} \cdot C_{lm} \tag{12}$$

$$\Delta\Phi_j^{i-1}/g = -\frac{\left(\Delta AL_{00}(t_j) + [RO_{00}(t_j)]^{i-1}\right)}{C_{00}} \tag{13}$$

where we have defined

$$RO_j^{i-1}(\theta,\phi) = \Delta\mathcal{SL}_j^{i-1}(\theta,\phi) \cdot C(\theta,\phi) \tag{14}$$

$$= \sum_{l,m} [RO_{lm}(t_j)]^{i-1} Y_{lm}((\theta,\phi) \tag{15}$$

While most of the calculations are done in the spherical harmonic domain, keeping this multiplication in the spatial domain simplifies the calculation and leads to the "pseudo" portion of the pseudo-spectral approach [*Mitrovica and Peltier*, 1991]. Thus equations (12), (13), and (11) are solved iteratively until ΔS converges.

[17] Appendix A lists a set of differences from *Kendall et al.* [2005], which details the full series of improvements to the sea level theory since *Farrell and Clark* [1976]. Many of these improvements are specifically relevant to the large ocean volume and topographic changes and presence of marine-based ice sheets during the last glacial cycle [e.g., *Johnston*, 1993; *Peltier*, 1994, 1998a, 1998b; *Milne et al.*, 1999; *Peltier and Drummond*, 2002].

3. Loads

[18] When considering the annual cycle in sea level, it is important to consider as many contributing factors as possible. Here, we implement a strategy similar to *Clarke et al.* [2005] and consider three sources of mass variations in and over the oceans: the global hydrological cycle, dynamic ocean variations, and changes in atmospheric pressure. When creating the forward-modeled time series, we consider the time span 1980–1997; 1980 is the first year for which both hydrological data sets are available (GLDAS/Noah starts in 1979), and HPD considered data only up to 1997. We consider each of these loads in turn.

3.1. Hydrology

[19] In this analysis, we have considered two global hydrology data sets: LadWorld-Gascoyne [*Milly and Shmakin*, 2002] and GLDAS/Noah [*Rodell et al.*, 2004]. An earlier version of LadWorld was used by *Milly et al.* [2003] to examine the sea level variations caused by this component. The GLDAS/Noah data set has been used in a number of studies that examine the GRACE data, as the hydrological cycle is the dominant cause for the observed gravity variations.

[20] For LadWorld-Gascoyne, we sum the data set's contributions from snow, water, and groundwater to find the total continental water storage. The total continental water storage from GLDAS/Noah is the sum of the snow water equivalent, the plant canopy surface water, and the four layers of soil moisture. While each of these data sets has missing components, they provide a good starting point for modeling the SAL effects of the hydrological cycle. Because we are only interested in the variations of sea level caused by changes in the continental water storage, we need only consider the variations from the time mean of this data set. Thus after adding the various contributions to the time series for every point on the data set grid, we remove a time-averaged value over the entire time span. We also mask out any contributions from Greenland and Antarctica (GLDAS/Noah only extends down to 60°S) as the snow values over each of these regions are unreliable.

[21] Given that the hydrological data sets do not specify the water storage in Greenland and Antarctica, we rectify this missing component by taking the annual and semiannual cycles estimated from data acquired by the GRACE satellite mission. These estimates are determined from simultaneous fits to an annual, semiannual, and quadratic polynomial in the GRACE time series for April 2002 through September 2008, after accounting for measurements errors and potential leakage from other geophysical signals as described by *Velicogna* [2009]. Separate time series are determined for northern and southern Greenland, as well as East and West Antarctica. In each case, we assume that the mass variation occurs uniformly over the region. While this method does suffer from the lack of geographic specificity present in the hydrological data sets, it will help to better determine the globally averaged amplitude and phase. Thus the results near Antarctica and Greenland may not be as accurate as desired, but in the far field this substitution should have little impact other than correcting the overall global amplitude and phase.

[22] The monthly values from each global grid are then interpolated to a Gauss-Legendre grid using bicubic interpolation. On this grid, we also apply an ocean mask determined from the ETOPO2v2 database [*U. S. Department of Commerce*, 2006] to consider contributions only over the continents. Then the load can easily be expanded in terms of spherical harmonics to degree and order 256 [e.g., *Sneeuw* 1994]. For future reference, we represent the hydrological component, ΔH, as

$$\Delta H(\theta,\phi,t_j) = \sum_{l,m} \Delta H_{lm}(t_j) Y_{lm}(\theta,\phi) \tag{16}$$

3.2. Ocean Bottom Pressure

[23] Changes in currents and water distribution within the ocean will also contribute to Earth loading, as well as gravitation variations. To quantify the impact of nontidal ocean loading, we have used the output from the MIT general circulation model simulation detailed in HPD. The results for this run are on a 1° × 1° grid with the domain extending over ±80° latitude. In particular, this model run was chosen due to the minimal data constraints applied during the run, with only the relaxation of surface salinity and temperature fields to observed climatological values. This helps avoid the possibility that SAL effects present in altimetry are incorrectly assimilated into the ocean model itself.

[24] As with the hydrological load, we remove a time-averaged (constant) value from the bottom pressure results

over 1980–1997 time span and interpolate to a Gauss-Legendre grid. Changes in the global average of the bottom pressure output are an artifact of the model's Boussinesq formulation [*Greatbatch*, 1994; *Ponte*, 1999] and not of changes in averaged atmospheric pressure or mass flux, which are not represented in the model. To correct for this effect, we subtract a uniform water layer over the entire ocean corresponding to the spatially averaged bottom pressure monthly value. If $\Delta PB_{lm}(t_j)$ are the spherical harmonic coefficients of ocean bottom pressure, converted to equivalent water height, then the equivalent water height used in total applied loads, $\Delta OBP_{lm}(t_j)$, would be

$$\Delta OBP_{lm}(t_j) = \Delta PB_{lm}(t_j) - \frac{\Delta PB_{00}(t_j)}{C_{00}} C_{lm} \tag{17}$$

Note that global average ΔOBP_{00} will be identically zero over time.

3.3. Atmospheric Pressure

[25] Incorporating atmospheric pressure into the calculations requires considering the different impacts of the load over the continents and oceans. At periods longer than 2 weeks, the ocean should respond statically as an inverted barometer (IB) to changes in pressure, P_a:

$$\eta^{ib} = -\left(\frac{P_a - \overline{P_a}}{\rho g}\right) \tag{18}$$

where $\overline{P}_a$ is the average atmospheric pressure over the ocean, ρ is the density of water, and g is gravity [e.g., *Ponte*, 1992; *Wunsch and Stammer*, 1997]. Thus the sea surface responds to counteract any changes in pressure, causing the loading of the Earth beneath the oceans to be a uniform value corresponding to $\overline{P}_a$. Studies of atmospheric loading generally assume that $\overline{P}_a$ is the only load associated with atmospheric variations over the oceans. *van Dam et al.* [1997] included the SAL impacts in this load (without the change in ocean mass discussed below) as well, showing that the maximum departure from the global average occurs near the continents.

[26] We use the monthly-mean surface pressure fields from the National Centers for Environmental Prediction/National Center for Atmospheric Research (NCEP/NCAR) reanalyses [*Kalnay et al.*, 1996] as the basis of the loading calculations. Given the discussion above, the original values of these fields are used over continents and the average atmospheric pressure over the oceans is distributed uniformly over the ocean. Thus we can express the total atmospheric load, $\Delta ATM_{lm}(t_j)$, as

$$\begin{aligned}\Delta PO(\theta,\phi,t_j) &= \Delta P(\theta,\phi,t_j)\cdot C(\theta,\phi) \\ &= \sum_{lm} \Delta PO_{lm}(t_j) Y_{lm}(\theta,\phi)\end{aligned} \tag{19}$$

$$\Delta ATM_{lm}(t_j) = \Delta P_{lm}(t_j) - \Delta PO_{lm}(t_j) + \frac{\Delta PO_{00}(t_j)}{C_{00}} C_{lm} \tag{20}$$

where ΔP is the initial atmospheric pressure field converted to water-equivalent height and ΔPO is the atmospheric pressure only over the oceans.

[27] In addition to these direct effects on sea level, the atmosphere indirectly affects sea level as it stores water in the form of water vapor. The dry component of atmospheric pressure is nearly constant, and thus the global average of surface pressure corresponds to changes in the water content of the atmosphere [*Trenberth and Smith*, 2005]. Consequently, part of this variation in the water content, $\Delta ATM_{00}(t_j)$, will contribute to a change in ocean mass.

3.4. Total Loads

[28] Above, we have described the process for arriving at each of the individual a priori components of the water cycle. However, none of these components accounts for water entering or leaving the oceans, and thus the water budget is not closed. Therefore in order to ensure a closed water budget, we assume that the deficit water at any given time t_j is provided by the oceans. We express $\Delta AL_{lm}(t_j)$ as

$$\Delta AL_{lm}(t_j) = \Delta H_{lm}(t_j) + \Delta ATM_{lm}(t_j) + \Delta OBP_{lm}(t_j) \tag{21}$$

Because the global average of the applied loads is balanced by the global average of the associated water load, we can write

$$\begin{aligned}\Delta S_{00}(t_j) &= -\Delta AL_{00}(t_j) \\ &= -\left(\Delta H_{00}(t_j) + \Delta ATM_{00}(t_j)\right)\end{aligned} \tag{22}$$

Here, we have explicitly removed ΔOBP_{00} because it is defined to be zero. As described earlier, this water will not be distributed uniformly because of both the crustal motion and changes in the sea surface. Therefore $\Delta AL_{lm}(t_j)$ is used in equation (11) and (13) during the iteration process. It should be noted again that our definition of SAL encompasses both the conservation of mass and geographic distribution of that mass throughout the oceans.

4. Comparing to Observations

[29] The results for the relative sea level (RSL) variations derived in section 2 represent motion of the sea surface relative to land, ignoring any direct effects of ocean dynamics, ocean density change, or atmospheric pressure change. In order to compare with tide gauge records, these effects must be added. For ocean dynamics and density changes, the sea level and ocean bottom pressure changes are obtained from the ocean model and can be added directly to ΔSL.

[30] The atmospheric pressure load requires special attention. For tide gauge measurements, the local sea surface is assumed to respond statically. Thus the IB response must be added to ΔSL when comparing to tide gauge data. Bottom pressure recorders measure the total mass of the column above them. Given the global definition of ΔSL, it would be equivalent to the change in ocean depth at any given location due to the inferred ocean load and mass redistribution. However, the direct impact of the atmospheric pressure on bottom pressure must still be considered. Therefore, given the discussion in section 3.3, bottom pressure records should

be compared to ΔSL plus the ocean-averaged atmospheric signal, $\overline{P}_a$.

5. Results

[31] To better illustrate the results, we will initially apply each of the loads separately. Thus for these preliminary results, we assume that the global average of each load is individually balanced by the inferred ocean load. Because the hydrological load has the largest contribution to the annual cycle of the inferred ocean load, we start by showing the best fitting annual phase and amplitude of GLDAS/Noah data over the period 1980–1997 together with the average annual cycle derived from the GRACE data over Greenland and Antarctica (Figure 1). The maximum of the water storage on the continents occurs during the Northern Hemisphere's winter (74°, the phase has been chosen so that 0° corresponds to 1 Jan). Note that the Amazon and Congo river basins are also in phase with most of the high and midlatitudes of the Northern Hemisphere. Given the assumed exchange of water between continents and oceans, the maximum of globally-averaged inferred ocean load would occur six months later (256°) than the continental water storage.

[32] Figure 3a shows the annual amplitude of resulting RSL. First, note that while the globally averaged annual amplitude is 10.5 mm, the amplitude varies spatially from less than 1.5 mm (less than 14% of the average) at some locations in the Arctic Ocean and the Gulf of Alaska to greater than 18 mm (a factor of over 1.7 times greater than the average) in the eastern boundary of the Bay of Bengal. This result can be understood by considering local effects in combination with the global average. The physics represented in Figure 2 indicates that during late winter when the loads are maximum in the high and midlatitudes of the Northern Hemisphere, as well as the Amazon and Congo basins, the SAL effect causes more water to be present in the ocean near these locations. However, at the same time the amount of water in the ocean is at its lowest levels. Thus the two effects nearly cancel, causing very small amplitudes near these continental regions. On the other hand, two effects are additive near southeast Asia and the central western coast of Africa. The water stored on land in these regions is at a maximum at the same time as the average ocean mass is at the maximum, and the resulting amplitudes are much larger than the global average.

[33] The phase of the RSL is shown in Figure 3b. Most of the oceans are in phase. The major exceptions are mainly in the Northern Hemisphere near the coasts. However, because the amplitudes are relatively small in these regions, it would be difficult to use the phase variation to uniquely identify this SAL effect in the tide gauge data.

[34] The variation in water moisture in the atmosphere is the next biggest contributor to the annual change in global mean RSL. Normally, when we consider the total load (equation (21)), water is exchanged among the continents, ocean and atmosphere. However, to illustrate the impact of SAL on the RSL change (Figure 4) we assume that water is only exchanged between the atmosphere and the oceans. The annual amplitude is 2.8 mm and has a phase of 21°. This is larger than the estimate of surface pressure variation in the work of *Trenberth and Smith* [2005] (~1.4 mm when converted to sea level), which was obtained from the European Centre for Medium-Range Weather Forecasts (ECMWF) Re-Analyses (ERA-40) pressure fields. However, these results are reasonable compared to their Figure 1. The annual amplitude reaches over 4.5 mm over much of Asia and Antarctica and exceeds 10 mm along the coasts of the Persian Gulf and the Yellow Sea. Note, however, that the total signal in the observations may be very different: the IB effect must be added to compare the results with tide gauge records and the globally averaged atmospheric pressure over the oceans must be added when comparing to bottom pressure measurements.

[35] By definition, the dynamic bottom pressure component has no globally averaged variation, and the globally average amplitude is zero. However, there is significant geographic variation in the SAL RSL component (Figure 5). The largest impacts are in the Gulf of Thailand and of Carpentaria, with amplitudes reaching over 10 mm, and in the Southern Indian Ocean, over 4 mm. These are regions where the largest annual cycles in ocean bottom pressure are found [*Ponte*, 1999; *Vinogradov et al.*, 2008].

[36] Finally, we add all of the contributions together to show ΔSL for the total load (Figure 6). Because the atmospheric freshwater component is 123° out of phase with the one due to hydrology, the globally averaged RSL amplitude is reduced to 9.1 mm with a phase of 268°. The spatial variation caused by the hydrological forcing (Figure 3) remains the dominant pattern in ΔSL for the total load. While the global amplitude is reduced, amplitudes along the coasts of the Bay of Bengal and central western Africa do not significantly decrease.

[37] To examine the impact of a different hydrological model on the results, we repeated the analysis using Lad-World-Gascoyne in place of GLDAS/Noah (while keeping the atmospheric and dynamic ocean loads the same). The results have a slightly larger globally averaged amplitude, 9.9 mm, and a slightly later phase, 274°. Taking into account the change in amplitude, the large-scale patterns of both models are very similar.

6. Comparison to Tide Gauge Records

[38] The global patterns shown in Figure 6 should be present in the tide gauge records. Thus we want to compare these modeled results, combined with the IB and ocean model time series, to the sea level variations derived from tide gauges. For this analysis, though, we utilize the entire time series from 1980 to 1997 so that interannual variations would also be captured. We start by showing the level of variability of the time series and then return to the study by HPD.

[39] Figure 7 shows the root-mean square (RMS) variability of the modeled time series about a time series constructed from the best-fitting annual, semiannual, trend and constant at each point shown on the map. For Figure 7, it is important to remember that we are only using monthly sampling. For the atmospheric forcing, in particular, this reduces the variability one might expect to see if finer samplings were used [e.g., *van Dam et al.*, 1997]. Atmospheric pressure variability contributes to the signal near Antarctica (the ocean model only extends to 80°S and the hydrological signal is defined to only have annual and

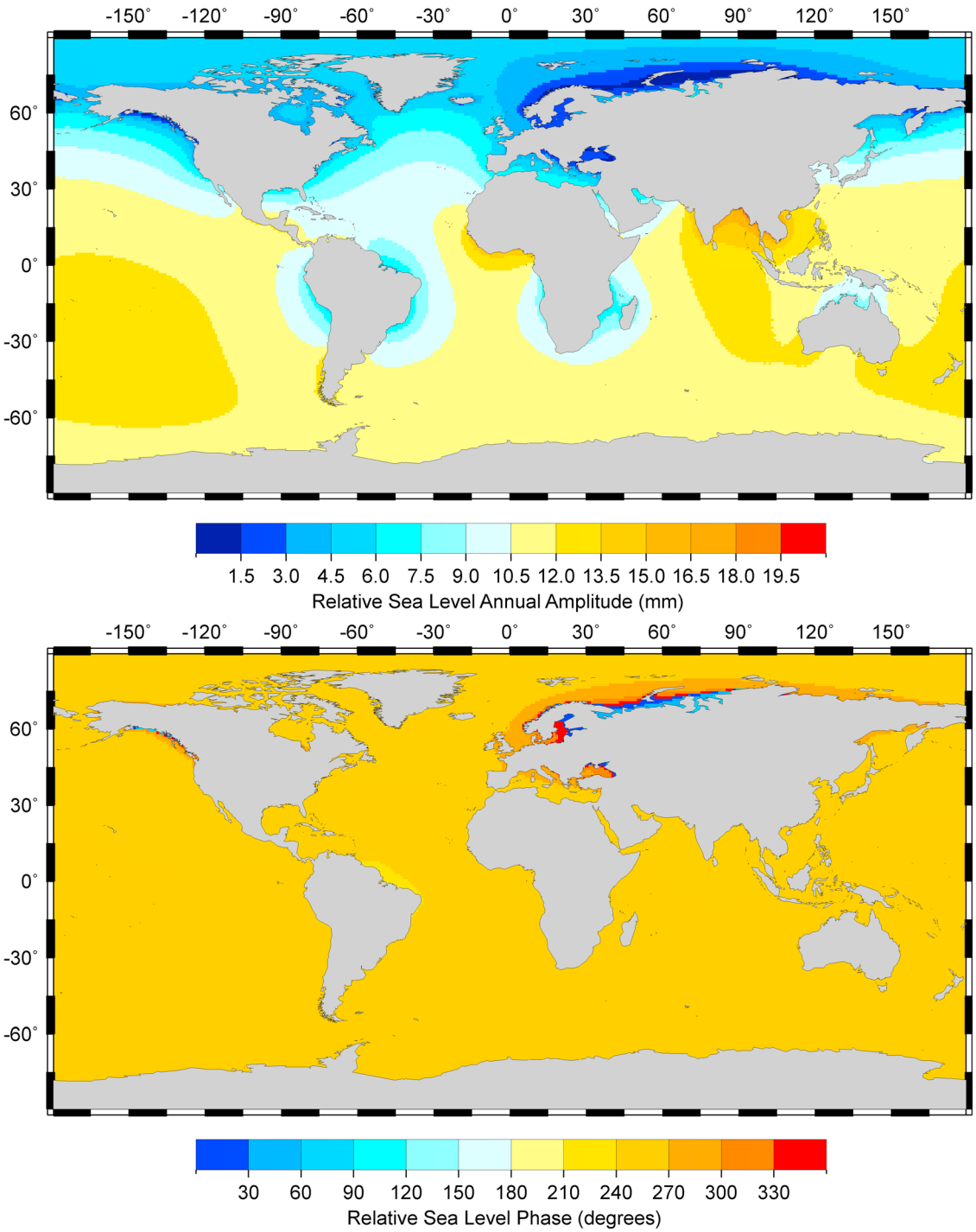

Figure 3. Annual-cycle (top) amplitude and (bottom) phase of the relative sea level caused by the hydrological load shown in Figure 1. The global average value is 10.5 mm and has a phase of 256°.

semiannual components.) Variability due to the dynamic ocean is seen in the southwestern Pacific and southwestern Indian oceans. Smaller-than-average RMS variability is seen near drier regions of northwestern Africa and the Arabian Peninsula. For the comparison with tide gauges, we will remove the best-fitting trend and constant from the modeled time series.

[40] HPD investigated the variance of the tide gauge time series explained by increasingly complex models of the sea level variation, comparing first to the time series derived from the IB effect and the ocean model and then also estimating an admittance parameter to the ocean model at each site to identify areas where scaling might be an issue. We continue this increasingly more detailed model comparison by including the impact of SAL. Specifically, we form two residual time series. The first, R_1, is the residual of the IB and scaled ocean model time series subtracted from the TG time series (this corresponds to R_{AOI} in HPD). The second,

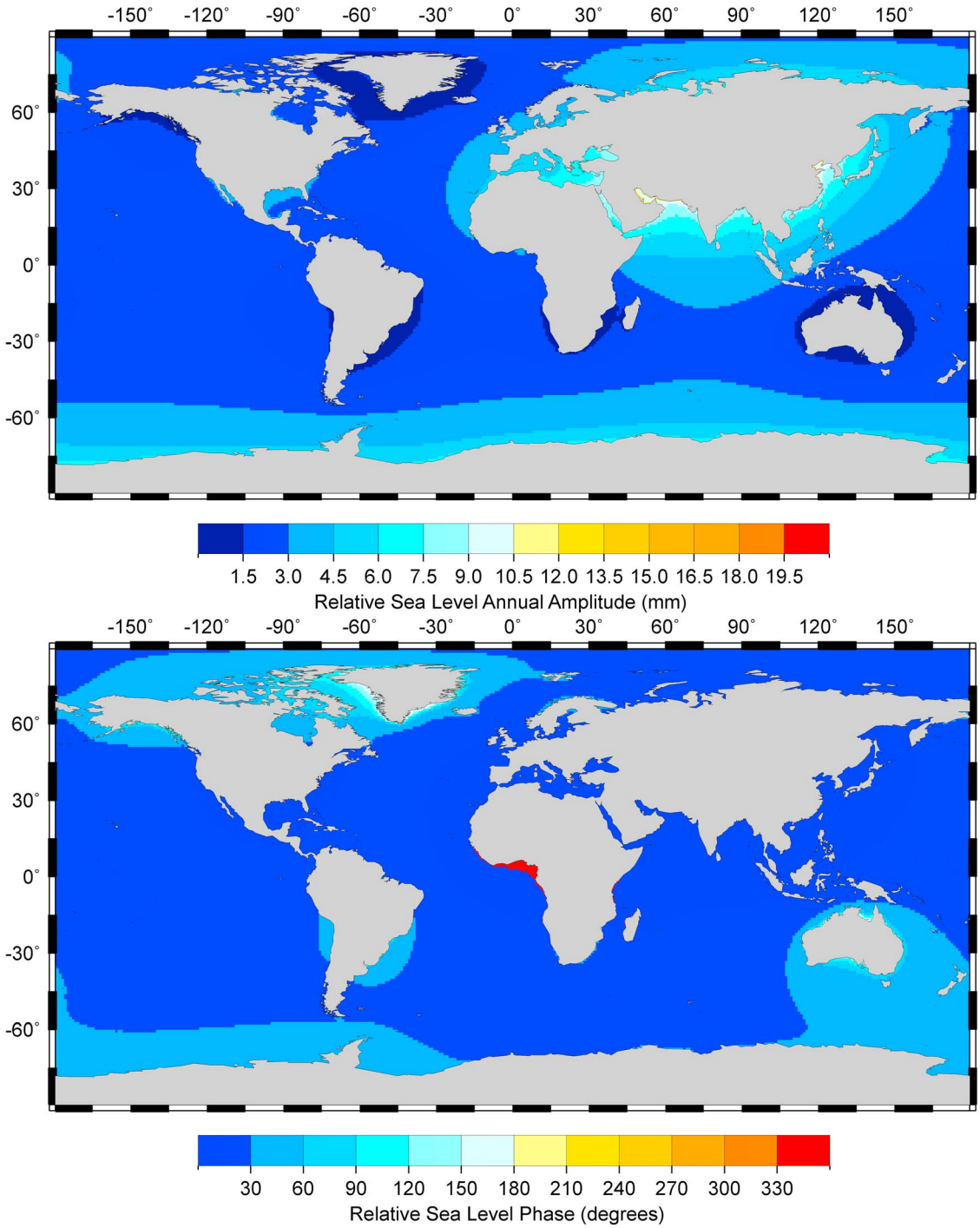

Figure 4. (top) Annual-cycle amplitude and (bottom) annual-cycle phase of the relative sea level caused by the atmospheric load, assuming the globally averaged variation in atmospheric pressure is caused by mass exchange only between the atmosphere and the oceans. The average amplitude is 2.8 mm and has a phase of 21°. While the amplitude is less than Figure 3, we will keep the same color bar in all of the following figures for comparison.

R_2, differs from R_1 by also having the SAL time series subtracted.

[41] We define the variance reduction as

$$\Delta^{v}_{1-2} = 100 \times \frac{\sigma_1^2 - \sigma_2^2}{\sigma_1^2}, \tag{23}$$

where σ_1^2 and σ_2^2 are the variances of the R_1 and R_2 time series. With this definition, an increase in variance when subtracting the SAL effects will be indicated by a negative number. Figure 8 shows Δ^{v}_{1-2} for 380 station records archived at the Permanent Service for Mean Sea Level [*Woodworth and Player*, 2003]. These records were chosen by HPD on the basis of having more than 20 years of data

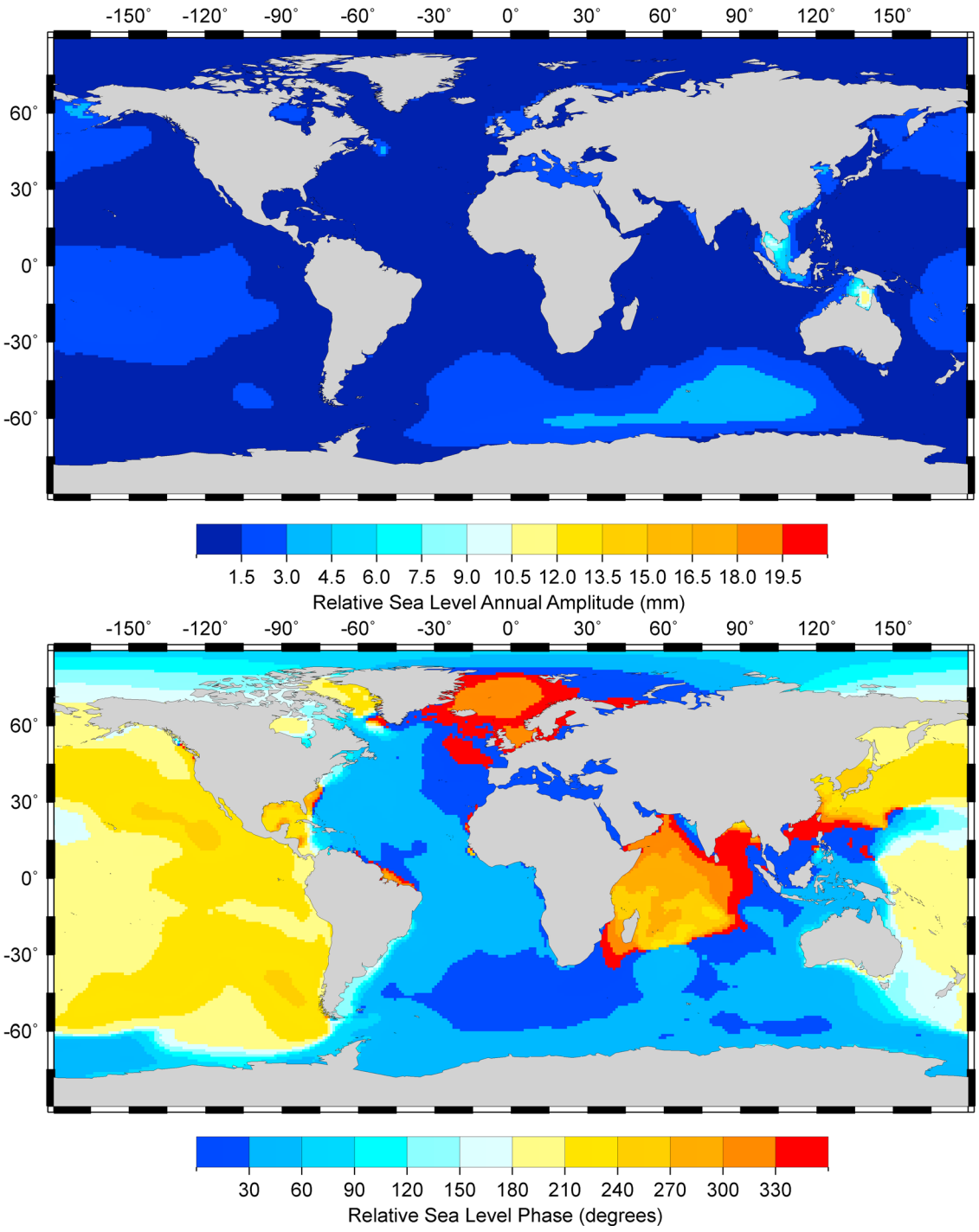

Figure 5. (top) Annual-cycle amplitude and (bottom) annual-cycle phase of the relative sea level caused by the the dynamic ocean bottom pressure. By definition, the global average is zero.

over the period 1958–1997, a longer time period than considered here. Overall, the variance reduction at the stations is positive, with an average value of 3.2%. However, there are distinct geographic patterns in the variance reduction. The introduction of the SAL effects reduces the variance of the time series along the North American east and west coasts, Europe, southeastern Asia, Africa, and Japan. Other locations see an increase in the variance: South American, Australia, and west central Pacific islands. In the case of Pacific island sites with particularly large increased variance, the tide gauge data show very little annual variation, whereas the annual amplitude of ΔSL is slightly larger than the global average. In South America, often the phase of R_1 and ΔSL are in disagreement.

[42] Because the ΔSL is particularly large in the Bay of Bengal, we have considered the variance reduction at ten tide gauge sites in that region. These 10 stations include four sites that were not part of the original 380 of the HPD

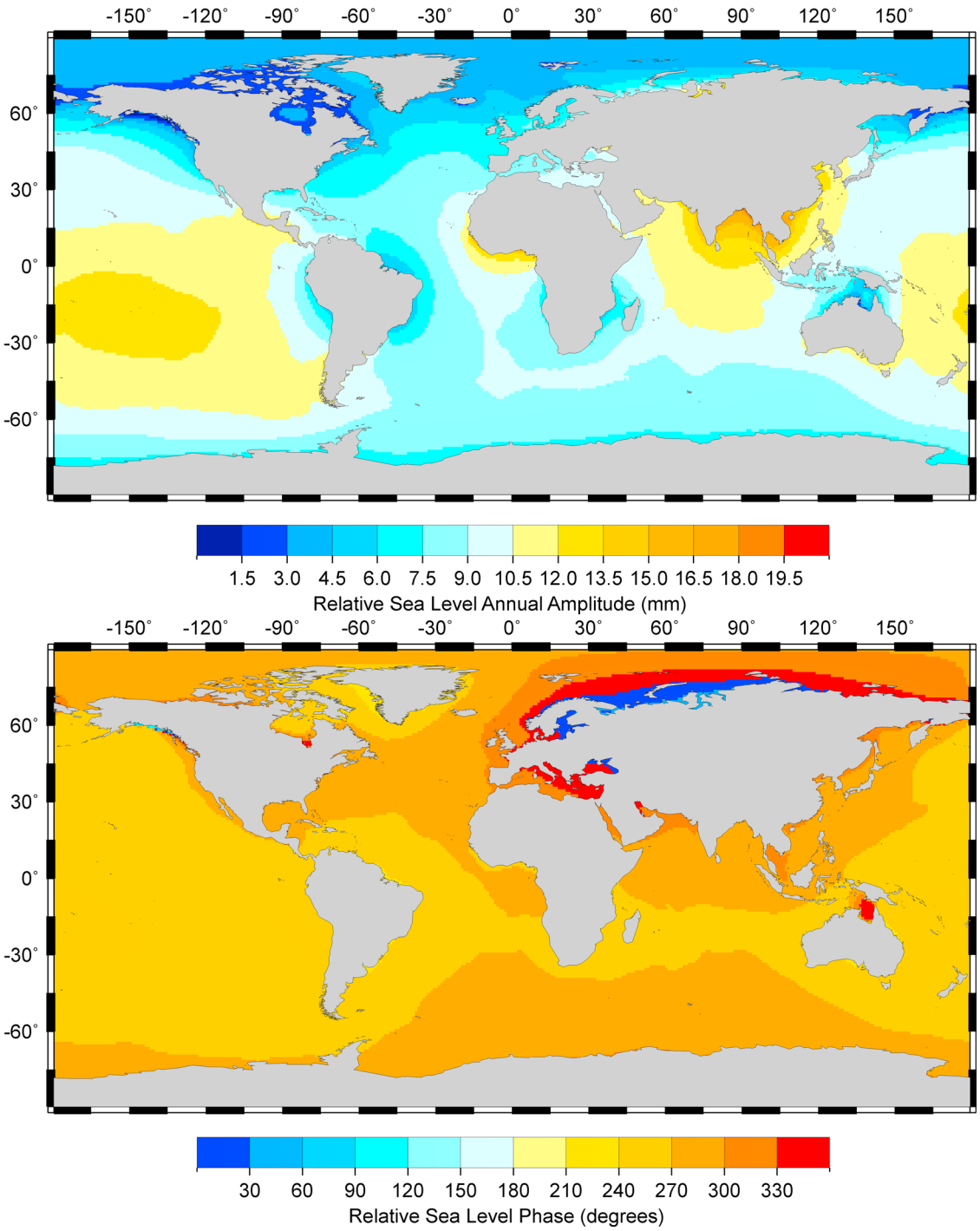

Figure 6. Annual-cycle (top) amplitude and (bottom) phase of the relative sea level caused by all the applied loads. The global average value has been reduced to 9.1 mm (compared to 10.5 mm of Figure 3) and has a phase of 268°. Note that this is the SAL effect and is not the total sea level variation. Rather the dynamic ocean signal and the inverted barometer effect must be added to compare to tide gauges.

analysis because they did not meet the original data requirements of that study. However, they did have very good coverage over the time span 1980–1997. At each tide gauge site, the variance is reduced across the region, with the average improvement of over 7% (see Table 1).

[43] Table 1 lists the average variance reduction, both globally and in the Bay of Bengal, for a number of different scenarios. The variance reduction in the Bay of Bengal is always larger than the global average. This is probably due to the much larger amplitude of ΔSL here than globally. However, one should also note that the annual amplitude of R_1 in the region is over 100 mm. Thus although SAL effects do not account for all of the residual annual cycle (which we did not expect; there are many other unmodeled effects that

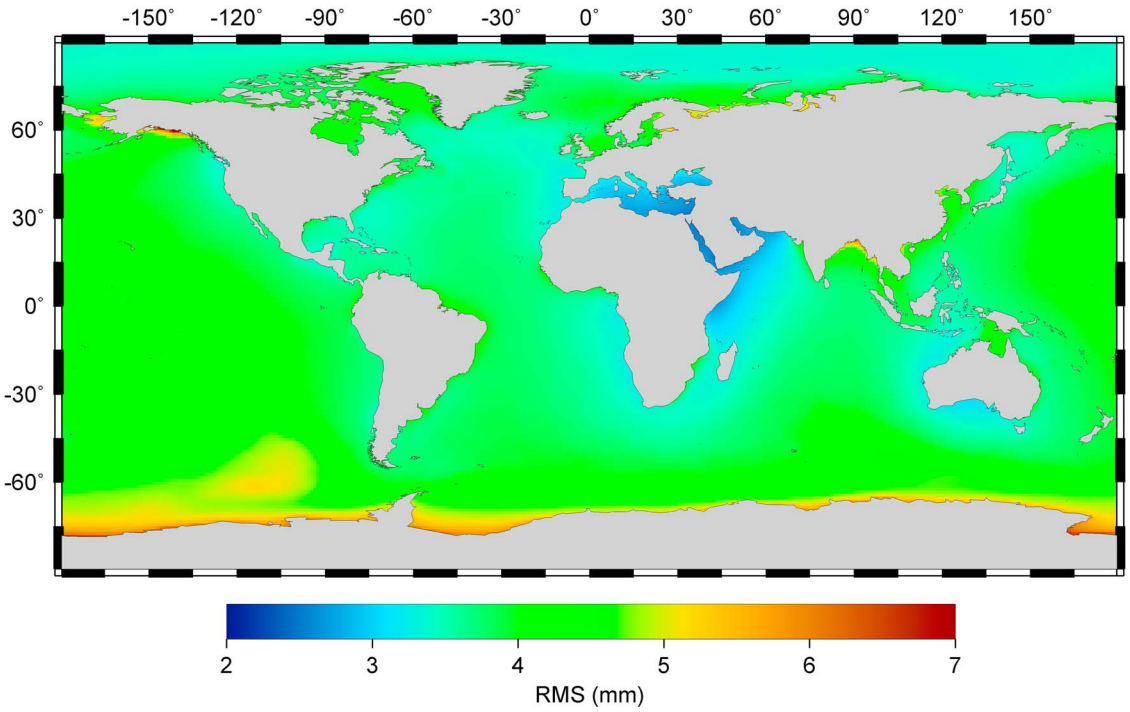

Figure 7. Root-mean-square (RMS) variation of the entire modeled time series about the best-fitting annual, semiannual, trend and constant for each location on the map.

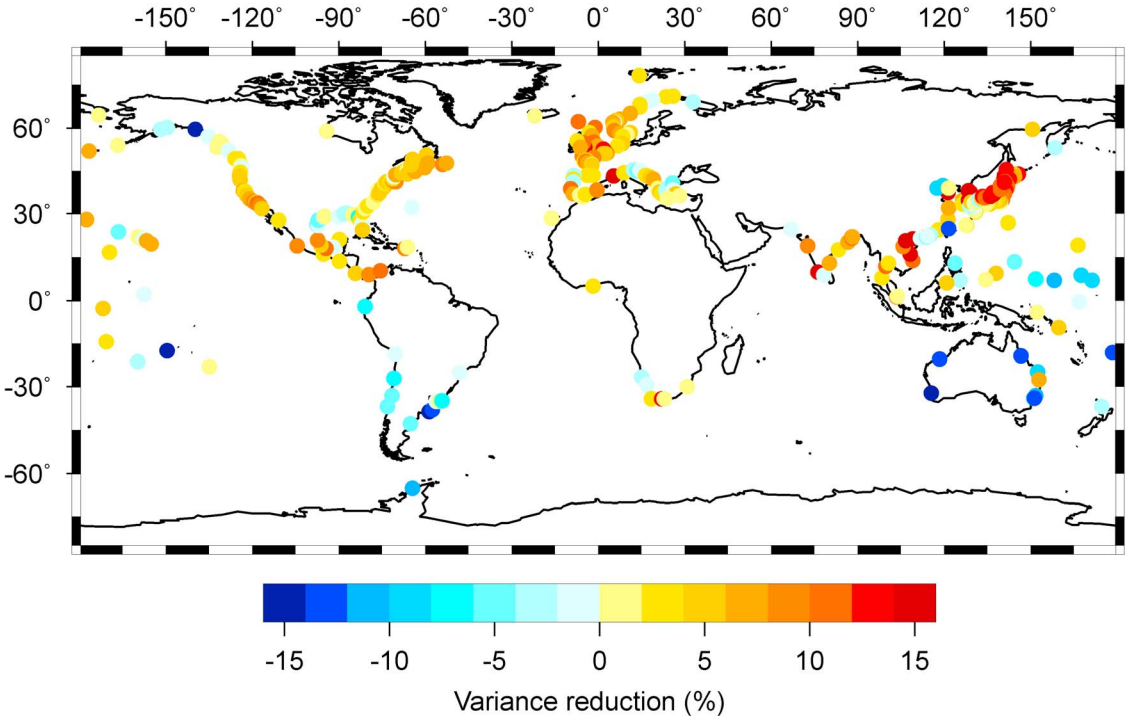

Figure 8. Percentage of variance reduction in the time series caused by removing derived ΔSL time series (the annual component of the time series is represented in Figure 6) from a time series of the tide gauge data with a scaled, dynamic ocean signal and inverted barometer removed (see Δ^{v}_{1-2} in text).

Table 1. Average Percentage of Variance Reduction[a]

	Global	Bay of Bengal
GLDAS	2.0	6.7
Total w/ GLDAS	3.2	7.2
LadWorld	2.9	7.2
Total w/ LadWorld	4.1	7.7

[a]Average percentage of variance reduction (see equation (23)) using either just the hydrological model with Greenland and Antarctica added or using the total load model (hydrological, atmospheric, and dynamic ocean bottom pressure.)

could contribute to this cycle), they comprise a significant signal that should not be ignored. Table 1 also lists the results of using just the hydrology model (GLDAS/Noah or LadWorld-Gascoyne) as the load. Both globally and in the Bay of Bengal, there is an increased variance reduction when including the atmospheric and dynamic ocean bottom pressure loads. This increase in variance reduction also illustrates that this effect is not driven simply by the amplitude of the modeled annual cycle because the annual amplitude decreases when all the processes in the water cycle are considered.

7. Conclusions

[44] We have calculated the SAL effects of the annual water cycle on tide gauge measurements. The results show that the effects of SAL have significant spatial variations, ranging from an amplitude of less than 1.5 mm to greater than 18 mm, similar to earlier studies [e.g., *Clarke et al.*, 2005]. Along many of the coasts in North America, Europe, northern Asia, and near the Congo and the Amazon basins, the annual cycle amplitudes of RSL will be less than the global average. At islands in the south central Pacific and along the coasts of west central Africa, and Southeast Asia, the amplitude will be greater than the average. In regions near Bangladesh, the response is nearly a factor of two greater. Thus in these regions, this effect becomes a significant one that must be considered when assimilating data into ocean models. It is also interesting to note that the SAL impact on sea level is at a maximum in the Bay of Bengal during the season when flooding is most likely to occur in Bangladesh.

[45] When comparing to tide gauge data, the introduction of the SAL effect improves the ability of an ocean model and IB time series to accurately predict the data. Starting with a residual time series (TG time series − scaled ocean model − IB time series), the global variance reduction obtained by removing the SAL effects is 3 to 4%, and in the Bay of Bengal variance reduction reaches 7 to 8%. Most of this reduction is associated with the annual cycle. These values of variance reduction, while small, are consistent with expectations. As discussed earlier, the annual amplitude of the globally averaged SAL effect amounts to about 25% of the average residual annual amplitude (35 mm) estimated by HPD, after accounting for a scaled ocean model and IB term as is done here. Furthermore, HPD found that the variance reduction of the tide gauge time series increased only from 60% to 71% when fitting and removing an annual cycle from the residual time series. Thus it is clear that the amount of variance explained by the SAL effects should be small. While there are many uncertainties in the modeled SAL effects presented here, the variance reduction is not expected to drastically increase with other hydrological data sets or SAL modeling techniques. Thus the most progress will be made by removing other, unrelated, signals that remain poorly modeled.

[46] There are a number of possible explanations for the remaining unexplained variability observed at the tide gauges, including measurement errors. Note that we have not removed the effects of the 14-month or annual pole tide [e.g., *Trupin and Wahr*, 1990; *Desai*, 2002], long-period equilibrium tides [e.g., *Egbert and Ray*, 2003], or atmospheric tides. However, the expected amplitudes of these effects are relatively small (e.g., the annual amplitudes are below 5 mm). More importantly, some tide gauges are near river outlets and may be greatly influenced, for example, by annual cycle in outflow [*Tsimplis and Woodworth*, 1994]. These and other factors can be poorly simulated in ocean models such as those used here.

[47] HPD address in detail many of the uncertainties associated with the global ocean model that may contribute to the unexplained variance in the TG records. Simulating sea level in coastal regions is difficult for global ocean models of coarse resolution. These models cannot adequately capture details of coastline geometry, bottom topography, near-coastal wind effects or forcing by river runoff, which can be important in determining the sea level observed at tide gauges. In addition, biases in the model physics and atmospheric boundary forcing make simulation of interannual variability a serious challenge. Thus improvement in the modeling of the coastal regions will probably lead to the largest improvements in the explanation of observed TG time series.

Appendix A

[48] *Mitrovica and Milne* [2003] give an extensive review of improvements in solving the sea level equation (SLE) and develop a unified theoretical approach which more easily and accurately incorporates the theory that lead to these improvements. *Kendall et al.* [2005, hereafter KMM] develop this theoretical approach into a practical algorithm for solving the SLE on spherically symmetric Earth models. The discussion presented in section 2 differs from KMM in several important ways. First, the history of the geometry and volume of the ice age oceans is much more involved than the simplified case considered here. We assume that the geometry of the oceans, represented by $C(\theta, \phi)$, is independent of time; that any ice sheets grounded in the ocean do not retreat or advance; and that the crustal motion is small enough to consider the topography to be time independent. As a practical consideration, the fact that the vertical resolution of the topography model (ETOPO2v2 [*U. S. Department of Commerce*, 2006]) is only in meters implies that the ~0.04 m peak-to-peak variation modeled here would not warrant considering a time varying coast line. However, KMM could not consider this simplification due to the much larger changes in sea level. In their algorithm C is time dependent, there is a function β which describes the presence or absence of ocean-grounded ice, and the time-varying topography (T) is explicitly considered. For example, compare

our equation (4) to KMM equation (3) and equation (7) to KMM equation (7).

[49] Second, in this paper we assume that the variations in the load will occur rapidly enough that the Earth will not deform in a viscous manner. Thus the time history of the loading and the Earth's response is unimportant. This is a significant difference from KMM. As a method of more easily expressing the changing load and Earth's response, KMM used δ to represent the change in some quantity between two time steps and Δ to represent the change from the beginning of loading. Given that we can assume an elastic response of the Earth, it is easiest to always express the changes of both the load and the Earth from its initial state, and therefore we always use Δ. This, combined with the simplifications described above, lead to the differences between our equation (8) and KMM equation (45) as well as our equation (9) and KMM equation (46). The elastic-response assumption also greatly simplifies the use of the viscoelastic Love number theory, so that KMM equation (B18) simplifies to our equation (11) by setting the viscous portion of the equation ($\beta^T(\ell, t_n, t_j)$) equal to zero.

[50] **Acknowledgments.** This study was funded by Natural Environment Research Council's Oceans 2025 program (MET), NASA grants NNX08AJ79G (EMH, JLD) and NNX07AM77G (EMH, RMP, JLD, NTV), NASA's Cryospheric Science Program, Solid Earth and Natural Hazards Program, Terrestrial Hydrology Program and the NSF Office of Polar Programs (IV). We would like to thank Chris Hughes for discussions and Erik Ivins and an anonymous reviewer for useful suggestions. The GLDAS/Noah data used in this study were acquired as part of the mission of NASA's Earth Science Division and archived and distributed by the Goddard Earth Sciences (GES) Data and Information Services Center (DISC). NCEP Reanalysis derived data were provided by the NOAA-ESRL PSD, Boulder, Colorado, USA, from their Web site at http://www.esrl.noaa.gov/psd/.

References

Blewitt, G., and P. Clarke (2003), Inversion of Earth's changing shape to weigh sea level in static equilibrium with surface mass redistribution, *J. Geophys. Res.*, *108*(B6), 2311, doi:10.1029/2002JB002290.

Cazenave, A., K. Dominh, S. Guinehut, E. Berthier, W. Llovel, G. Ramillien, M. Ablain, and G. Larnicol (2009), Sea level budget over 2003–2008: A reevaluation from GRACE space gravimetry, satellite altimetry and Argo, *Global Planet. Change*, *65*, 83–88.

Chambers, D. P., J. Wahr, and R. S. Nerem (2004), Preliminary observations of global ocean mass variations with GRACE, *Geophys. Res. Lett.*, *31*, L13310, doi:10.1029/2004GL020461.

Clark, J. A., and J. A. Primus (1987), Sea-level changes resulting from future retreat of ice sheets: An effect of CO_2 warming of the climate, in *Sea-Level Change*, edited by M. J. Tooley and I. Shennan, pp. 256–370, Inst. of Brit. Geogr., London.

Clarke, P. J., D. A. Lavallée, G. Blewitt, T. M. van Dam, and J. M. Wahr (2005), Effect of gravitational consistency and mass conservation on seasonal surface mass loading models, *Geophys. Res. Lett.*, *32*, L08306, doi:10.1029/2005GL022441.

Conrad, C., and B. H. Hager (1997), Spatial variations in the rate of sea level rise caused by present-day melting of glaciers and ice sheets, *Geophys. Res. Lett.*, *24*, 1503–1506.

Desai, S. D. (2002), Observing the pole tide with satellite altimetry, *J. Geophys. Res.*, *107*(C11), 3186, doi:10.1029/2001JC001224.

Egbert, G. D., and R. D. Ray (2003), Deviation of long-period tides from equilibrium: Kinematics and geostrophy, *J. Phys. Oceanogr.*, *33*, 822–839.

Farrell, W. E., and J. A. Clark (1976), On postglacial sea level, *Geophys. J. R. Astron. Soc.*, *46*, 647–667.

Greatbatch, R. J. (1994), A note on the representation of steric sea level in models that conserve volume rather than mass, *J. Geophys. Res.*, *99*, 12,767–12,771.

Hill, E. M., R. M. Ponte, and J. L. Davis (2007), Dynamic and regression modeling of ocean variability in the tide-gauge record at seasonal and longer periods, *J. Geophys. Res.*, *112*, C05007, doi:10.1029/2006JC003745.

Johnston, P. (1993), The effect of spatially non-uniform water loads on predictions of sea level change, *Geophys. J. Int.*, *114*, 615–634.

Kalnay, E., et al. (1996), The NCEP/NCAR 40-year reanalysis project, *Bull. Am. Meteorol. Soc.*, *77*, 437–470.

Kendall, R. A., J. X. Mitrovica, and G. A. Milne (2005), On post-glacial sea level – II. Numerical formulatioin and comparative results on spherically symmetric models, *Geophys. J. Int.*, *161*, 679–706, doi:10.1111/j.1365-246X.2005.02553.x.

Leuliette, E. W., and L. Miller (2009), Closing the sea level rise budget with altimetry, Argo, and GRACE, *Geophys. Res. Lett.*, *36*, L04608, doi:10.1029/2008GL036010.

Milly, P. C. D., A. Cazenave, and M. C. Gennero (2003), Contribution of climate-driven change in continental water storage to recent sea-level rise, *Proc. Natl. Acad. Sci.*, *100*, 13,158–13,161, doi:10.1073/pnas.2134014100.

Milly, P. C. D., and A. B. Shmakin (2002), Global modeling of land water and energy balances. Part I: The land dynamics (LaD) model, *J. Hydrometeorology*, *3*, 283–299.

Milne, G. A., J. X. Mitrovica, and J. L. Davis (1999), Near-field hydro-isostasy: The implementation of a revised sea-level equation, *Geophys. J. Int.*, *139*, 464–482.

Mitrovica, J. X., and G. A. Milne (2003), On post-glacial sea level: I. General theory, *Geophys. J. Int.*, *154*, 253–267.

Mitrovica, J. X., and W. R. Peltier (1991), On postglacial geoid subsidence over the equatorial oceans, *J. Geophys. Res.*, *96*, 20,053–20,071.

Mitrovica, J. X., M. E. Tamisiea, J. L. Davis, and G. A. Milne (2001), Recent mass balance of polar ice sheets inferred from patterns of global sea-level change, *Nature*, *409*, 1026–1029.

Nakiboglu, S. M., and K. Lambeck (1991), Secular sea-level change, in *Glacial Isostasy, Sea-Level and Mantle Rheology*, edited by R. Sabadini, K. Lambeck, and E. Boschi, pp. 237–258, Kluwer Acad., Dordrecht, Netherlands.

Peltier, W. R. (1994), Ice age paleotopography, *Science*, *265*, 195–201.

Peltier, W. R. (1998a), Postglacial variations in the level of the sea: Implications for climate dynamics and solid-Earth geophysics, *Rev. Geophys.*, *36*, 603–689.

Peltier, W. R. (1998b), "Implicit ice" in the global theory of glacial isostatic adjustment, *Geophys. Res. Lett.*, *25*, 3955–3958.

Peltier, W. R., and R. Drummond (2002), A "broad-shelf effect" upon post-glacial relative sea level history, *Geophys. Res. Lett.*, *29*(8), 1169, doi:10.1029/2001GL014273.

Plag, H.-P., and H.-U. Jüttner (2001), Inversion of global tide gauge data for present-day ice load changes, in *Proceedings of the Second International Symposium on Environmental Research in the Arctic and Fifth Ny-Alesund Scientific Seminar*, vol. 54, pp. 301–318, Natl. Inst. of Polar Res., Tokyo.

Ponte, R. M. (1992), The sea level response of a stratified ocean to barometric pressure forcing, *J. Phys. Oceanogr.*, *22*, 109–113.

Ponte, R. M. (1999), A preliminary model study of the large-scale seasonal cycle in bottom pressure over the global ocean, *J. Geophys. Res.*, *104*, 1289–1300.

Ponte, R. M. (2006), Low frequency sea level variability and the inverted barometer effect, *J. Atmos. Oceanic Technol.*, *23*, 619–629.

Ponte, R. M., K. J. Quinn, C. Wunsch, and P. Heimbach (2007), A comparison of model and GRACE estimates of the large-scale seasonal cycle in ocean bottom pressure, *Geophys. Res. Lett.*, *34*, L09603, doi:10.1029/2007GL029599.

Ray, R. D. (1998), Ocean self-attraction and loading in numerical tidal models, *Mar. Geod.*, *21*, 181–192.

Rodell, M., J. S. Famiglietti, J. Chen, S. I. Seneviratne, P. Viterbo, S. Holl, and C. R. Wilson (2004), Basin scale estimates of evapotranspiration using GRACE and other observations, *Geophys. Res. Lett.*, *31*, L20504, doi:10.1029/2004GL020873.

Sneeuw, N. (1994), Global spherical harmonic analysis by least-squares and numerical quadrature methods in historical perspective, *Geophys. J. Int.*, *118*, 707–716.

Tamisiea, M. E., J. X. Mitrovica, G. A. Milne, and J. L. Davis (2001), Global geoid and sea-level changes due to present-day ice mass fluctuations, *J. Geophys. Res.*, *106*, 30,849–30,864.

Trenberth, K. E., and L. Smith (2005), The mass of the atmosphere: A constraint on global analyses, *J. Clim.*, *18*, 864–875.

Trupin, A., and J. Wahr (1990), Spectroscopic analysis of global tide gauge sea level data, *Geophys. J. Int.*, *100*, 441–453.

Tsimplis, M. N., and P. L. Woodworth (1994), The global distribution of the seasonal sea level cycle calculated from coastal tide gauge data, *J. Geophys. Res.*, *99*, 16,031–16,039.

U. S. Department of Commerce (2006), 2-minute gridded global relief data (ETOPO2v2), Washinton, D. C. (Available at http://pubs.usgs.gov/of/2006/1150/metadata/bathymetry.htm)

van Dam, T. M., J. Wahr, Y. Chao, and E. Leuliette (1997), Predictions of crustal deformation and of geoid and sea-level variability caused by oceanic and atmospheric loading, *Geophys. J. Int.*, *129*, 507–517.

Velicogna, I. (2009), Increasing rates of ice mass loss from the Greenland and Antarctic ice sheets revealed by GRACE, *Geophys. Res. Lett.*, *36*, L19503, doi:10.1029/2009GL040222.

Vinogradov, S. V., R. M. Ponte, P. Heimbach, and C. Wunsch (2008), The mean seasonal cycle in sea level estimated from a data-constrained general circulation model, *J. Geophys. Res.*, *113*, C03032, doi:10.1029/2007JC004496.

Vinogradova, N. T., R. M. Ponte, M. E. Tamisiea, J. L. Davis, and E. M. Hill (2010), Effects of self-attraction and loading on annual variations of ocean bottom pressure, *J. Geophys. Res.*, *115*, C06025, doi:10.1029/2009JC005783.

Willis, J. K., D. P. Chambers, and R. S. Nerem (2008), Assessing the globally-averaged sea level budget on seasonal to interannual timescales, *J. Geophys. Res.*, *113*, C06015, doi:10.1029/2007JC004517.

Woodworth, P. L., and R. Player (2003), The Permanent Service for Mean Sea Level: An update to the 21st century, *J. Coastal Res.*, *19*, 287–295.

Wu, X., M. B. Heflin, E. R. Ivins, and I. Fukumori (2006), Seasonal and interannual global surface mass variations from multisatellite geodetic data, *J. Geophys. Res.*, *111*, B09401, doi:10.1029/2005JB004100.

Wunsch, C., and D. Stammer (1997), Atmospheric loading and the oceanic "inverted barometer" effect, *Rev. Geophys.*, *35*, 79–107.

J. L. Davis and E. M. Hill, Harvard-Smithsonian Center for Astrophysics, 60 Garden St., Cambridge, MA 02138, USA.

R. M. Ponte and N. T. Vinogradova, Atmospheric and Environmental Research, Inc., 131 Hartwell Ave., Lexington, MA 02421, USA.

M. E. Tamisiea, National Oceanography Centre, Joseph Proudman Bldg., 6 Brownlow Street, Liverpool, L3 5DA, UK. (mtam@pol.ac.uk)

I. Velicogna, School of Physical Sciences, University of California, Irvine, CA 92697, USA.